Electronic Supplementary Material (ESI) for RSC Advances.

Supporting Information

A step forward in the development of SOD mimetic nanozymes: the effect of the charge of the surface on antioxidant activity

Álvaro Martínez-Camarena, José M. Llinares, Antonio Domenech-Carbó, Javier Alarcón, Enrique García-España.

Contents

I. Figures

Figure S40. Fitting of the SOD activity data obtained by the McCord-Fridovich method for the system Cu_2-**SNP-L1**.

Figure S41. Fitting of the SOD activity data obtained by the McCord-Fridovich method for the system Cu_2-**SNP-L2**.

Figure S42. Representation of the catalytic constant corresponding to the systems: a) Cu-**L5**, Cu-**L6**, Cu-**L7**, Cu-**L8**, Cu_2-**L3**, Cu_2-**L1**, Cu_2-**L2**, Cu_2-**L9**, Cu_2-**L10**, Cu_2-**L4**, Cu_2-**SNP-L1**, Cu_2-**SNP-L2**, Cu_2-**BNP-L2**, Cu_2-**BNP-L1**.[1-3]

Figure S43. Representation of the variation of the absorbance intensity with time at 219 nm for H_2O_2 solutions with the presence of the ligands, both functionalised an free in solution. Yellow line corresponds to the EUK-134 reference.[1]

II. Tables.

Table S1. Concentration of the grafted ligand, Cu^{2+} complexation capability and ζ-potential values determined for the different nanoparticle systems. All measurements were carried out in 10^{-4} M $NaClO_4$ at pH 7.4.

Table S2. Logarithms of the stepwise protonation constants for **L3** and **L4** obtained by potentiometric measurements.[1] The constants were determined in 0.15 M $NaClO_4$ at 298.1 ± 0.1 K.

Table S3. Logarithm of the equilibrium constants for the interaction of Cu^{2+} with **L3** and **L4** obtained by potentiometric measurements.[1] The logarithms constants were determined in 0.15 M $NaClO_4$ at 298.1 ± 0.1 K.

Table S4. Logarithms of the equilibrium constants for the interaction of Zn^{2+} with **L1** and **L2** obtained by potentiometric measurements. The logarithms constants were determined in 0.15 M $NaClO_4$ at 298.1 ± 0.1 K.

Table S5. Logarithm of the equilibrium constants for the interaction of Zn^{2+} with **L3** and **L4** obtained by potentiometric measurements.[1] The logarithms constants were determined in 0.15 M $NaClO_4$ at 298.1 ± 0.1 K.

Table S6. Logarithm of the equilibrium constants for the interaction of Cu^{2+} and Zn^{2+} with **L3** and **L4** obtained by potentiometric measurements.[1] The logarithms constants were determined in 0.15 M $NaClO_4$ at 298.1 ± 0.1 K.

III. References.

I. Figures

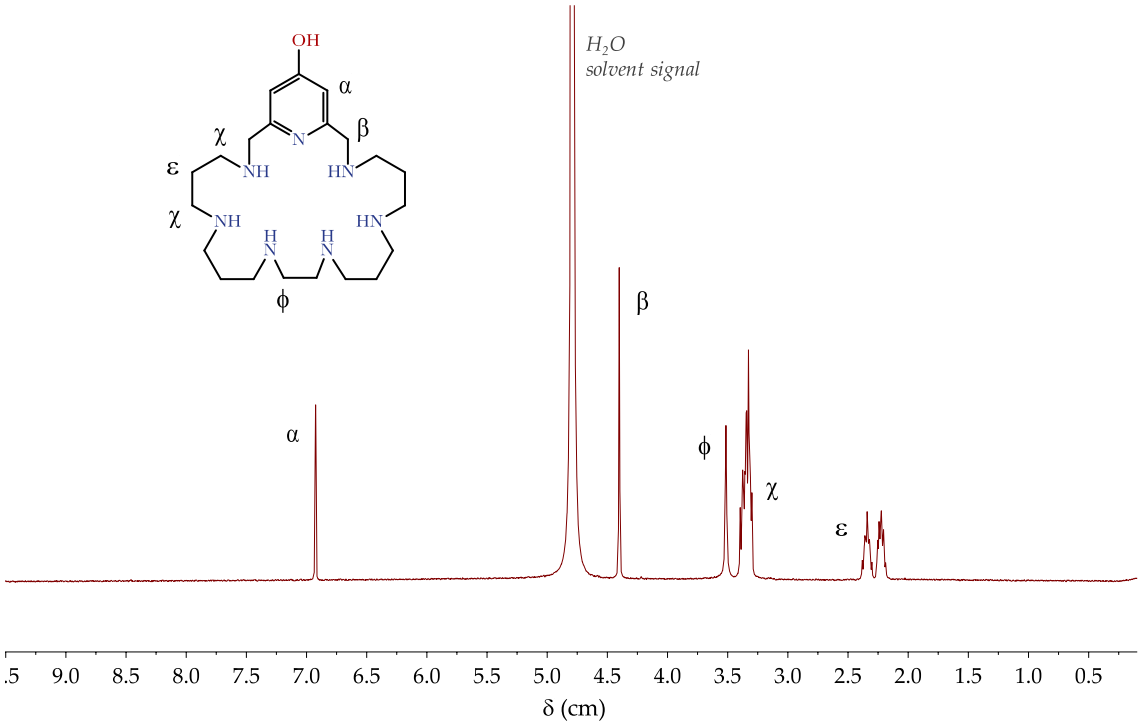

Figure S1. 1H-NMR spectrum of **L1** in D2O at 298 K.

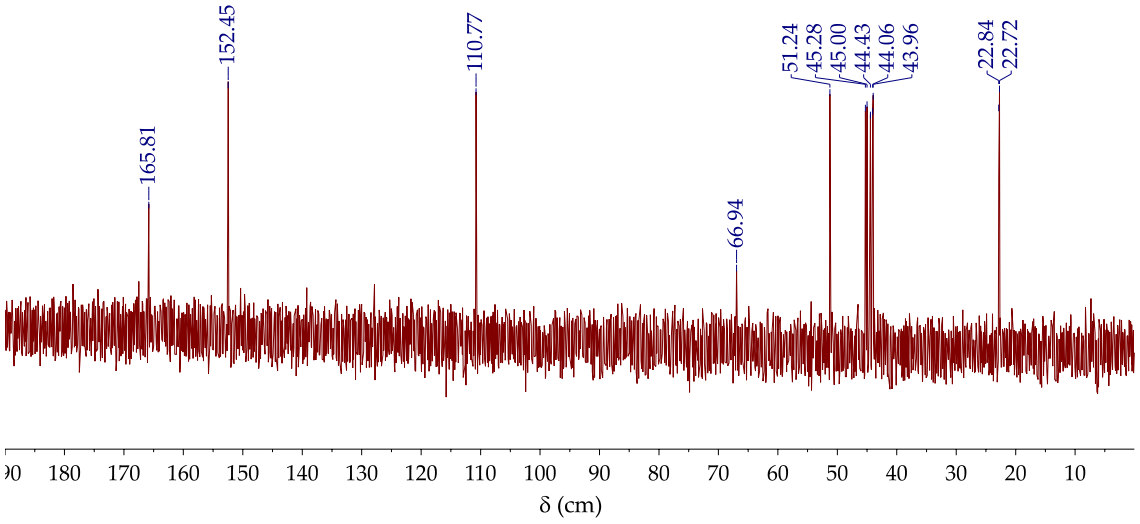

Figure S2. 13C-NMR spectrum of **L1** in D2O at 298 K.

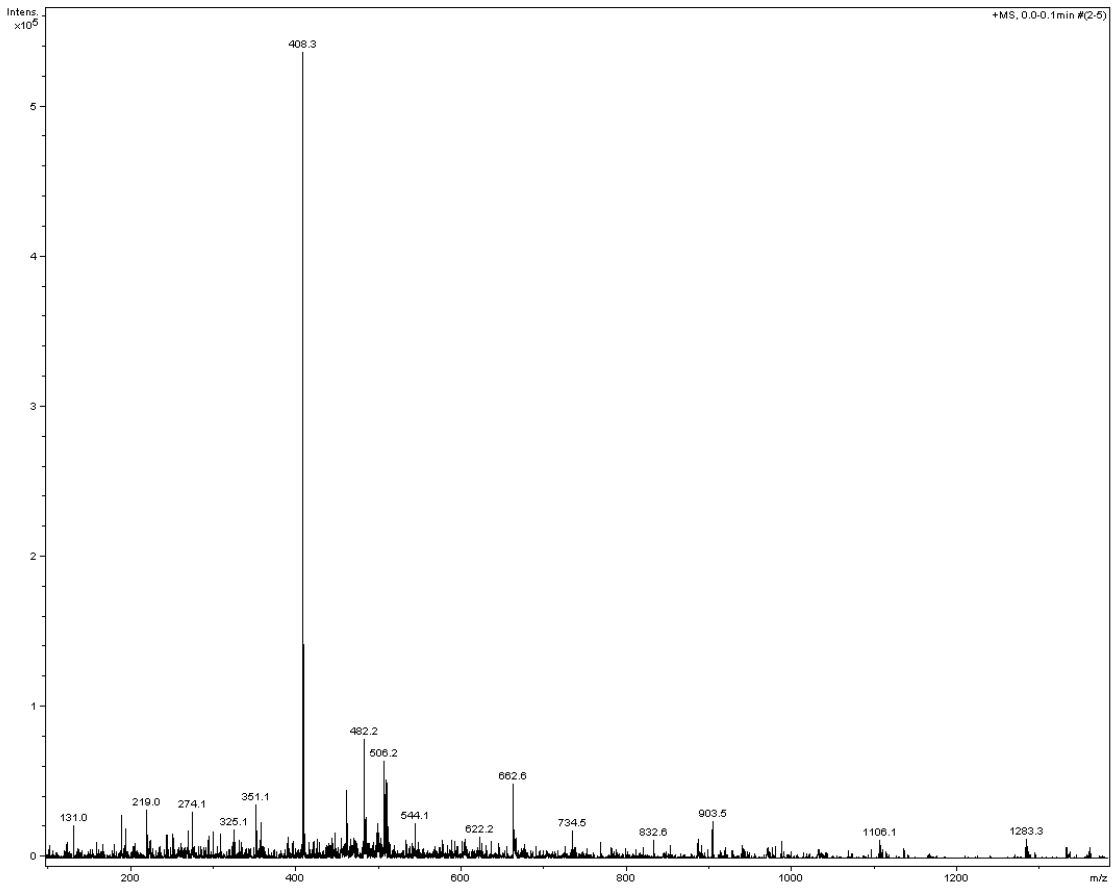

Figure S3. Mass spectrum of **L1**.

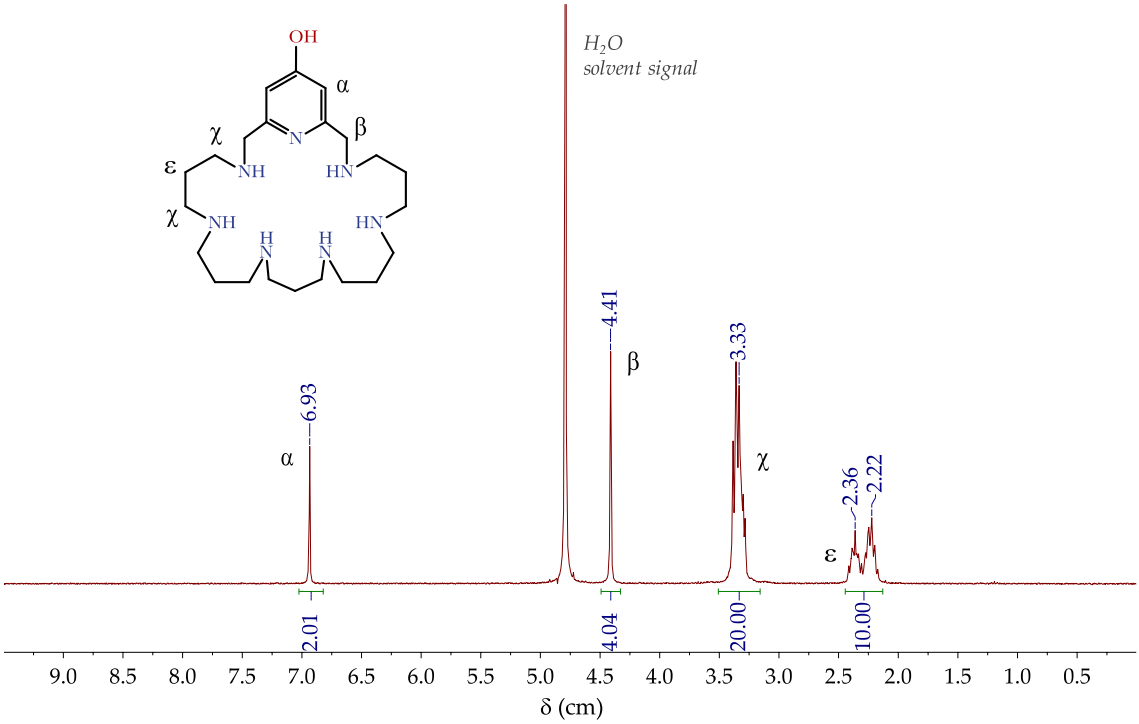

Figure S4. 1H-NMR spectrum of **L2** in D2O at 298 K.

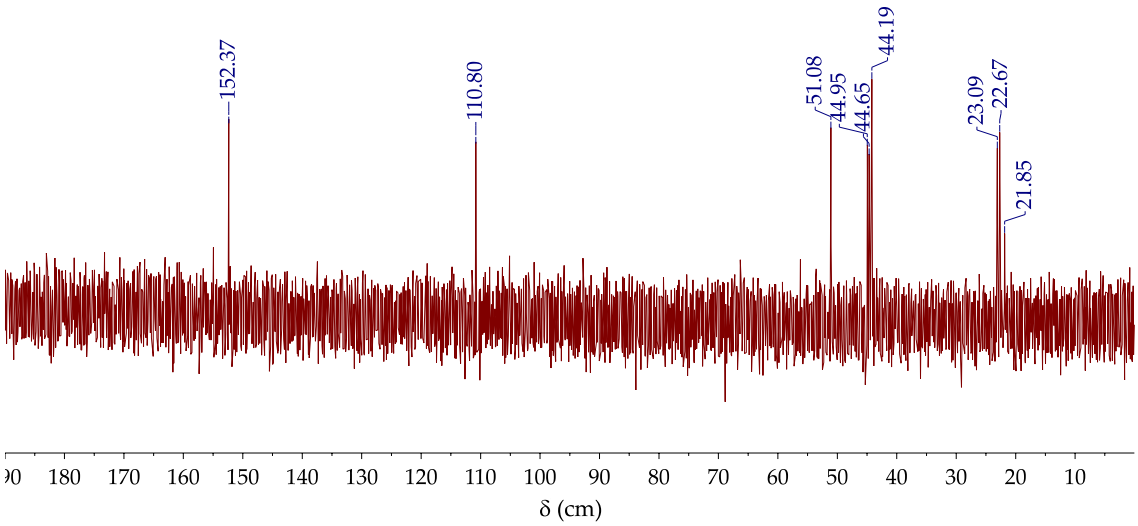

Figure S5. ^{13}C-NMR spectrum of **L2** in D_2O at 298 K.

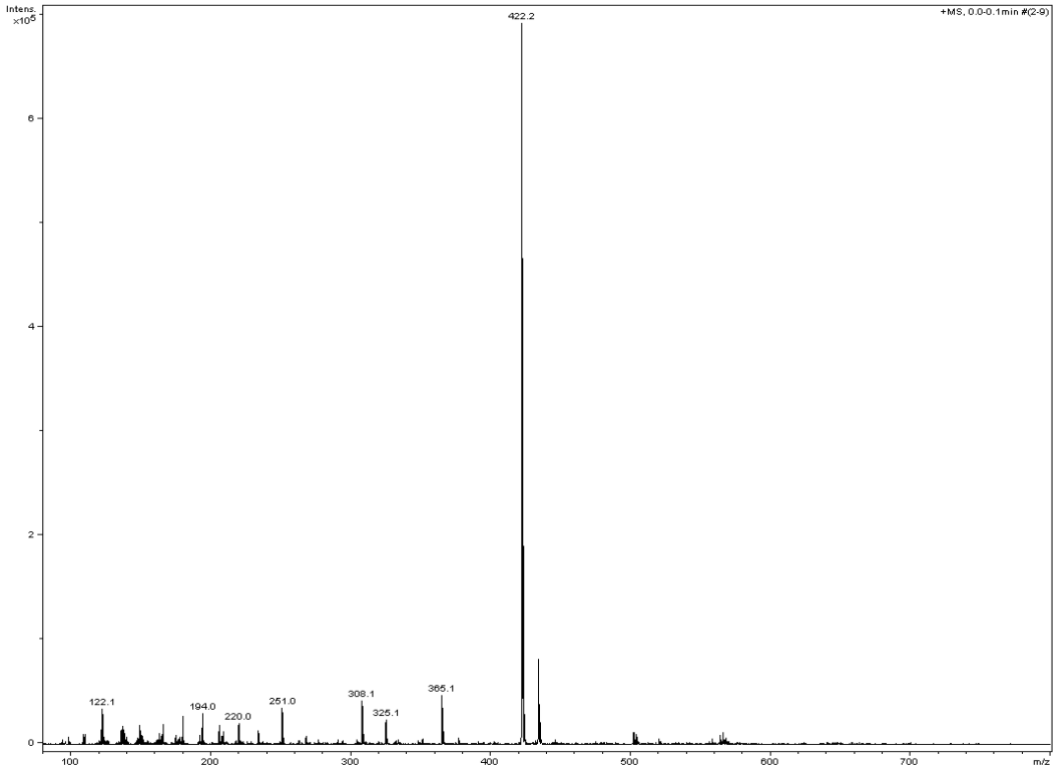

Figure S6. Mass spectrum of **L2**.

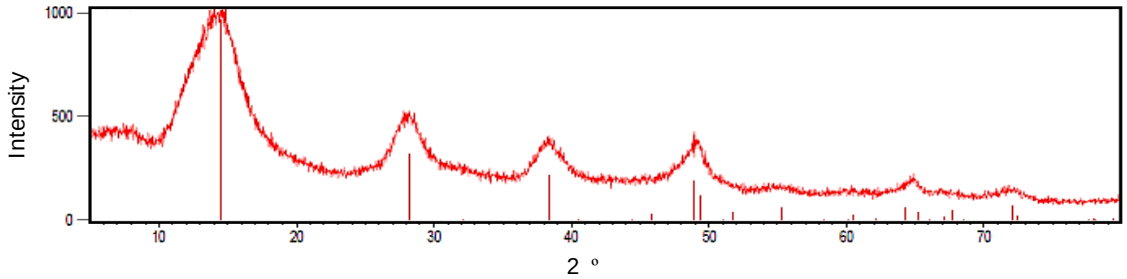

Figure S7. Experimental (red, continuous line) and theoretical (discrete red peaks) diffractogram of the boehmite nanoparticles powder.

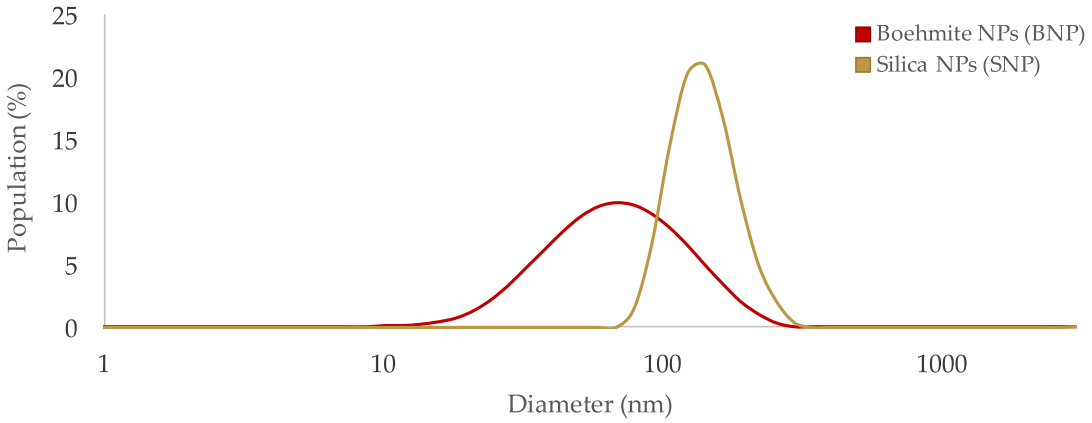

Figure S8. Size dispersion diagram of the boehmite nanoparticles obtained by DLS.

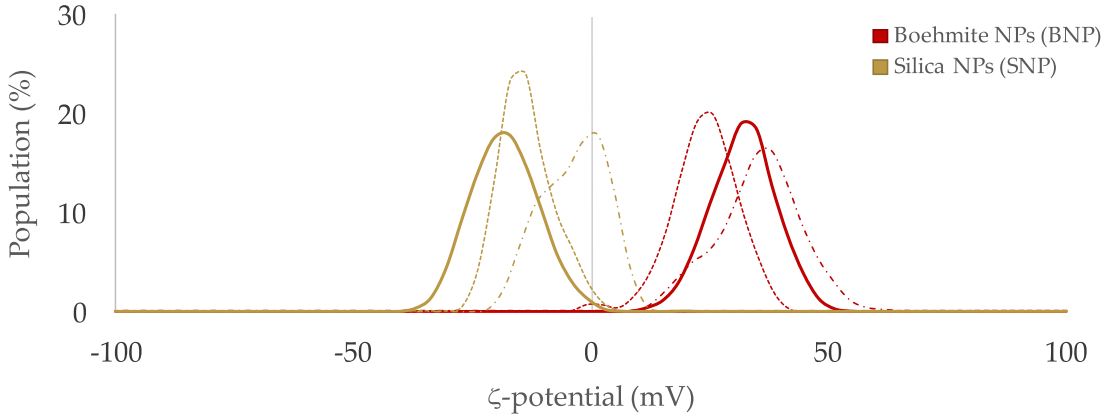

Figure S9. Experimental ζ-potential of the oxidic nanoparticles. The continuous lines correspond to the non-functionalised nanoparticles, while the dotted lines correspond to the NPs functionalised with **L1** and the dotted-dashed ones to the NPs functionalised with **L2**.

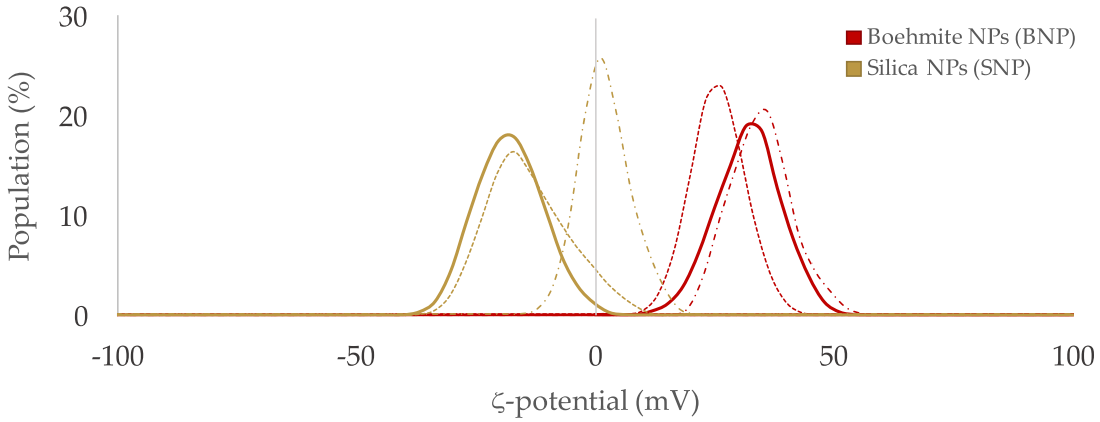

Figure S10. Experimental ζ-potential of the oxidic nanoparticles. The continuous lines correspond to the non-functionalised nanoparticles, while the dotted lines correspond to the NPs functionalised with Cu_2**L1** and the dotted-dashed ones to the NPs functionalised with Cu_2**L2**.

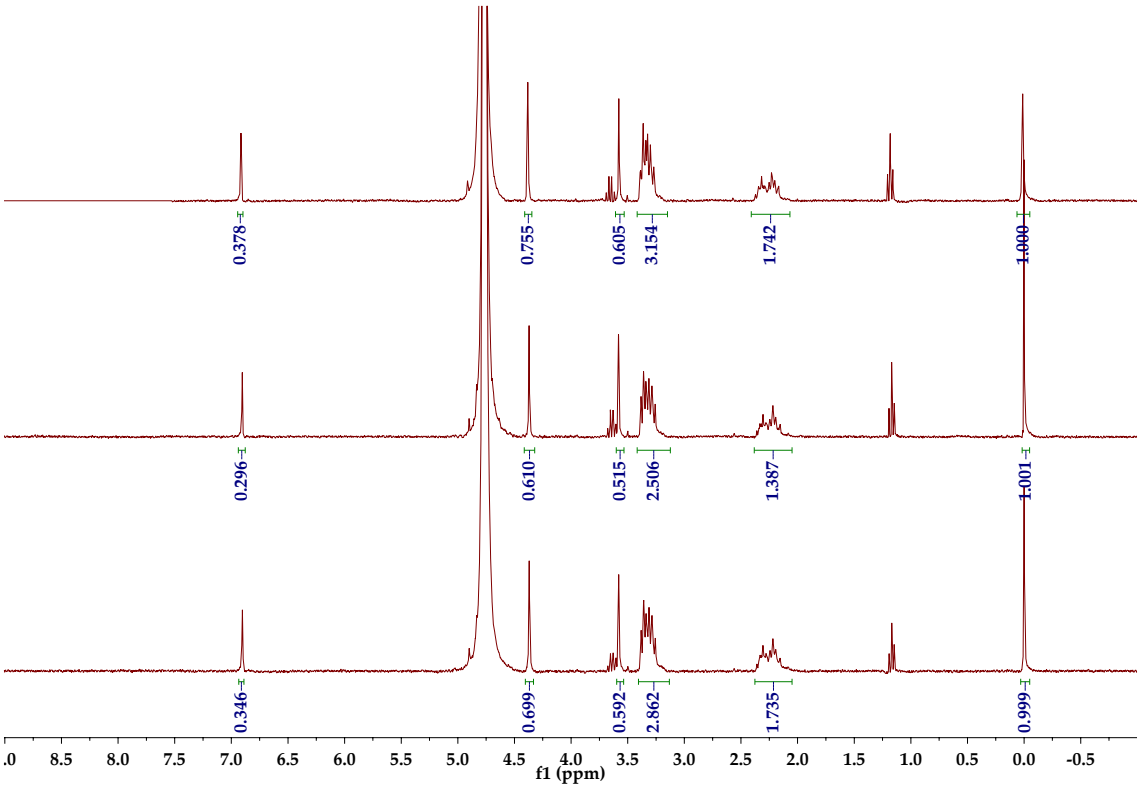

Figure S11. ^{1}H-NMR spectra of the three BNP-**L1** samples in D_2O at 298 K.

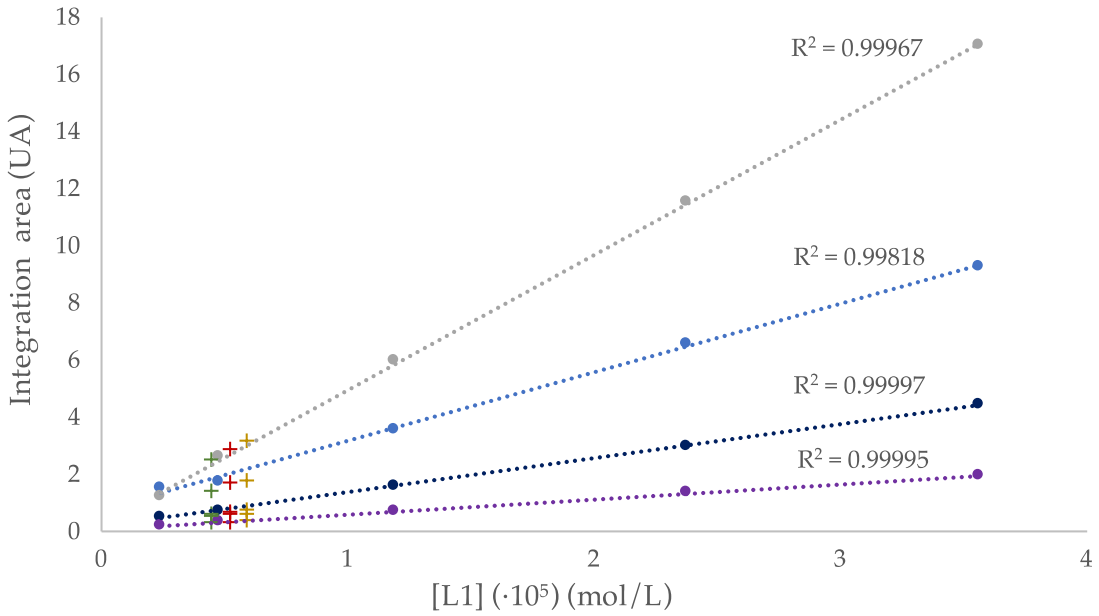

Figure S12. Calibration and interpolation of **L1** anchoring to boehmite nanoparticles by NMR determination.

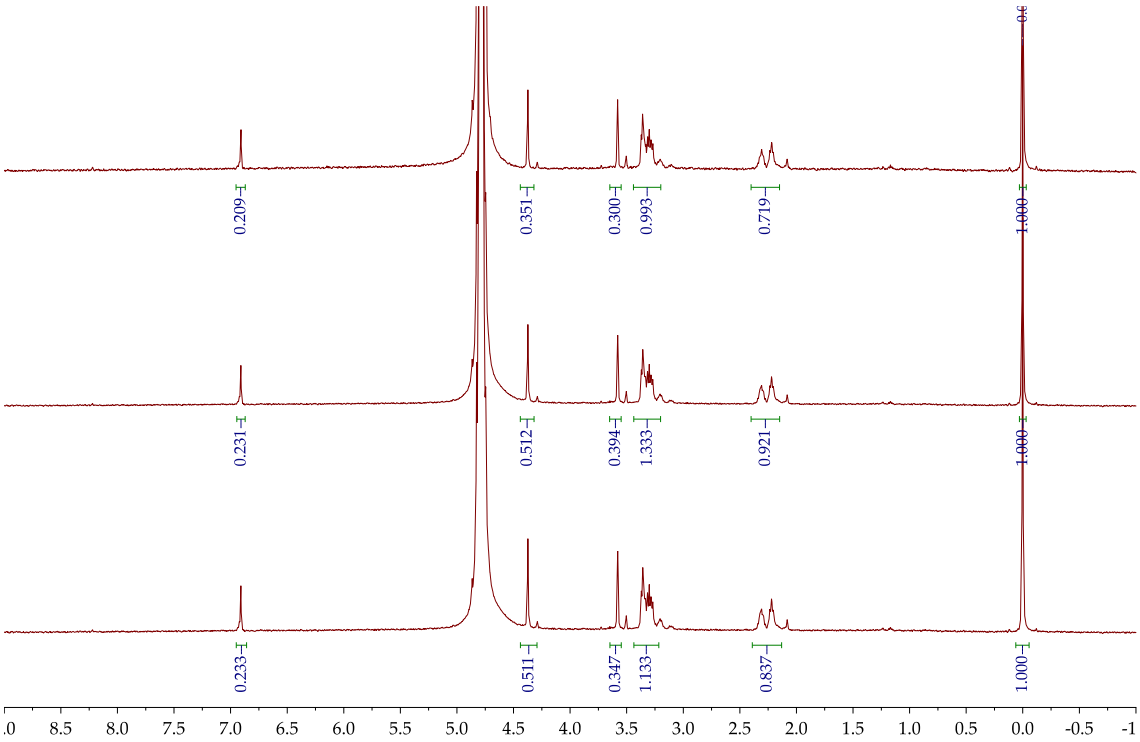

Figure S13. 1H-NMR spectra of the three SNP-**L1** samples in D_2O at 298 K.

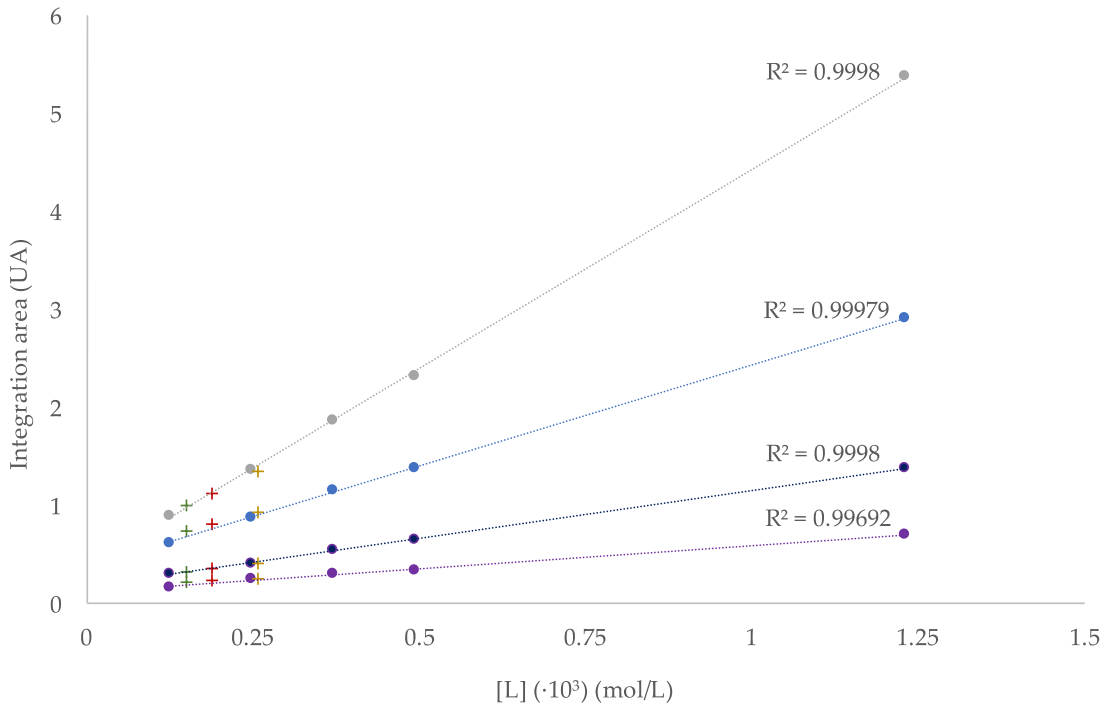

Figure S14. Calibration and interpolation of **L1** anchoring to silica nanoparticles by NMR determination.

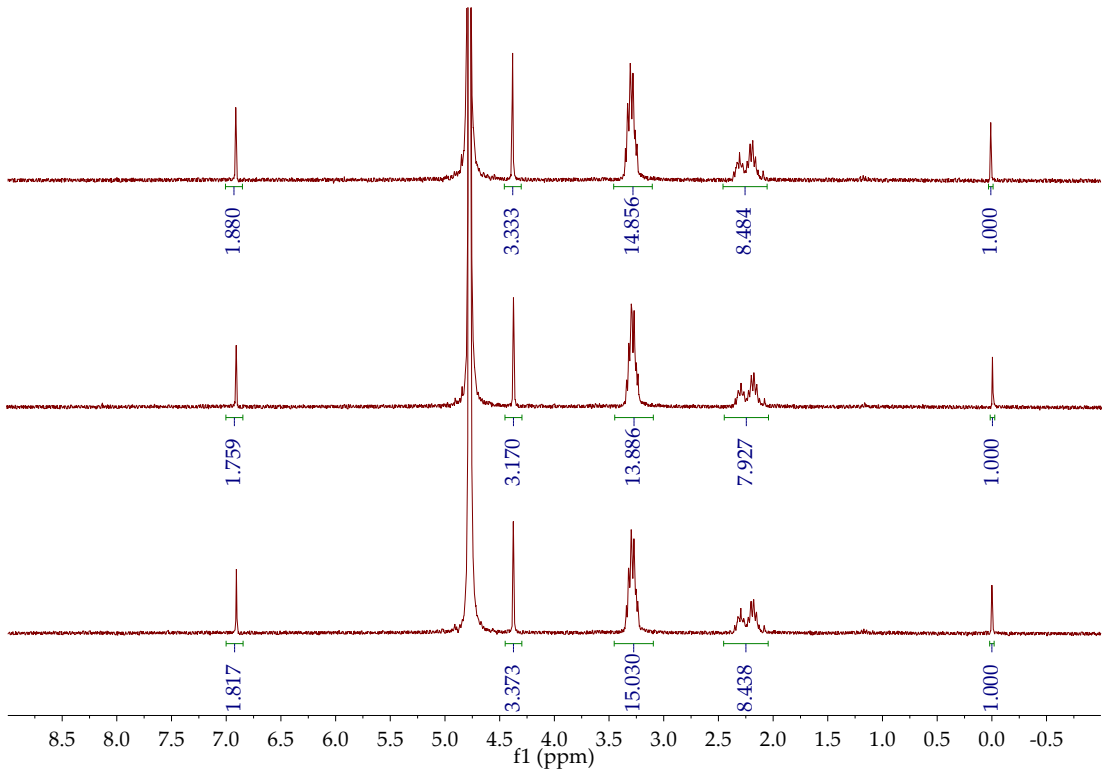

Figure S15. 1H-NMR spectra of the three BNP-**L2** samples in D_2O at 298 K.

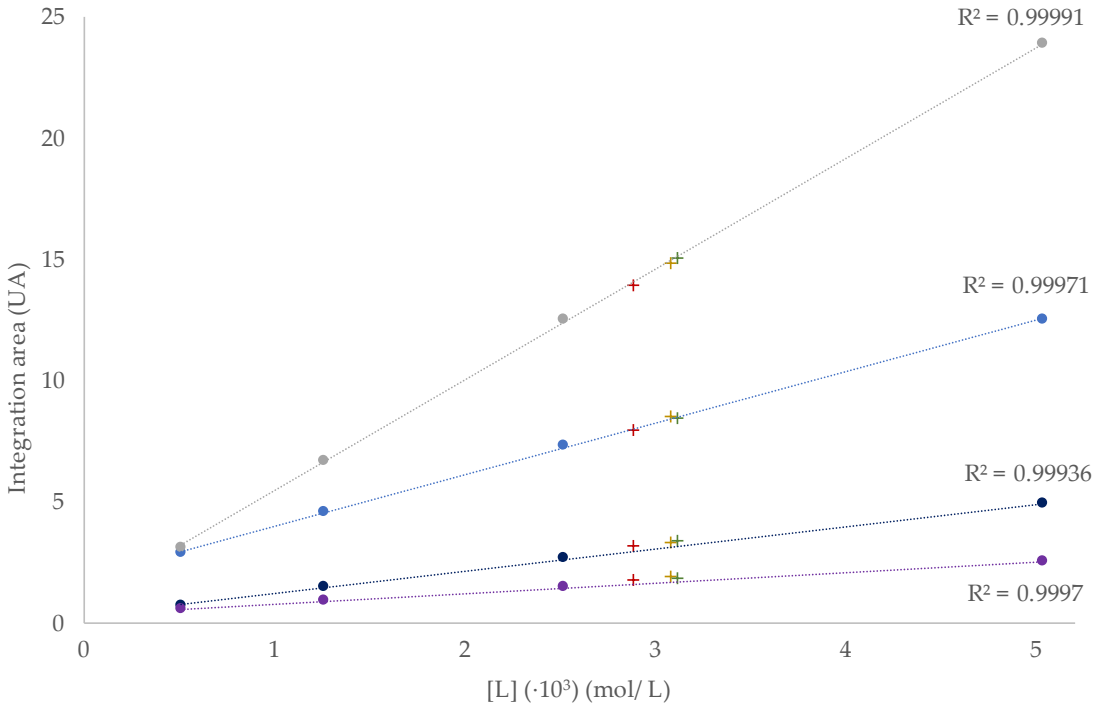

Figure S16. Calibration and interpolation of **L2** anchoring to boehmite nanoparticles by NMR determination.

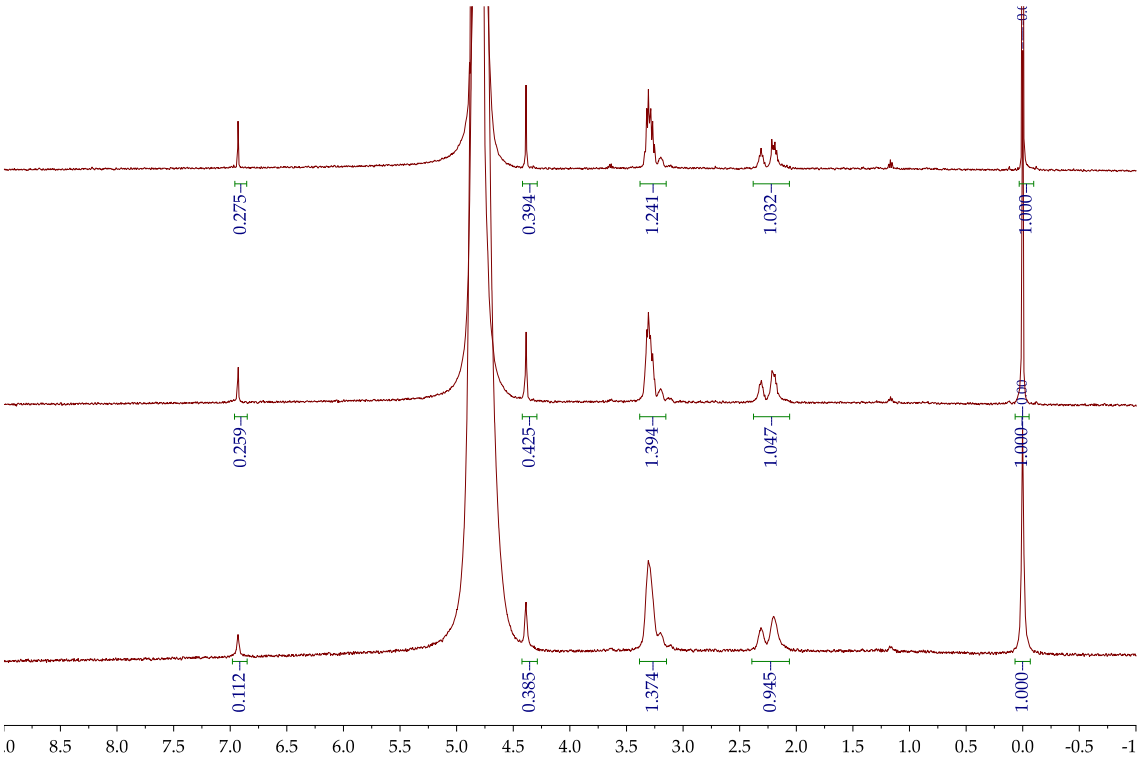

Figure S17. ^{1}H-NMR spectra of the three SNP-**L2** samples in D_2O at 298 K.

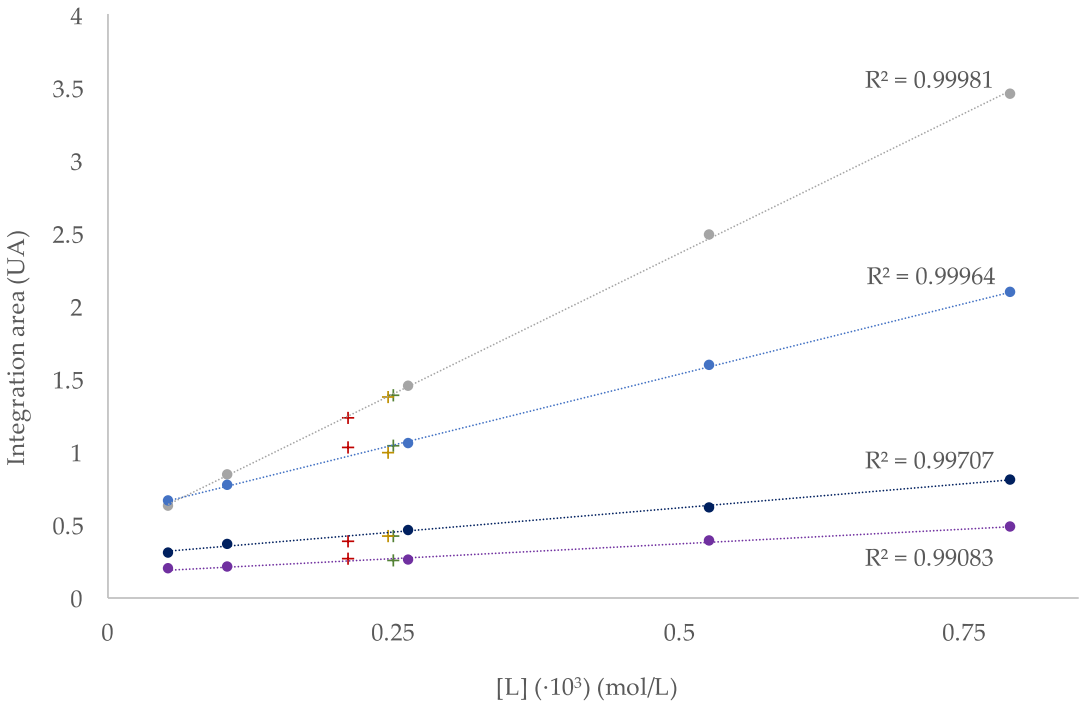

Figure S18. Calibration and interpolation of **L2** anchoring to silica nanoparticles by NMR determination.

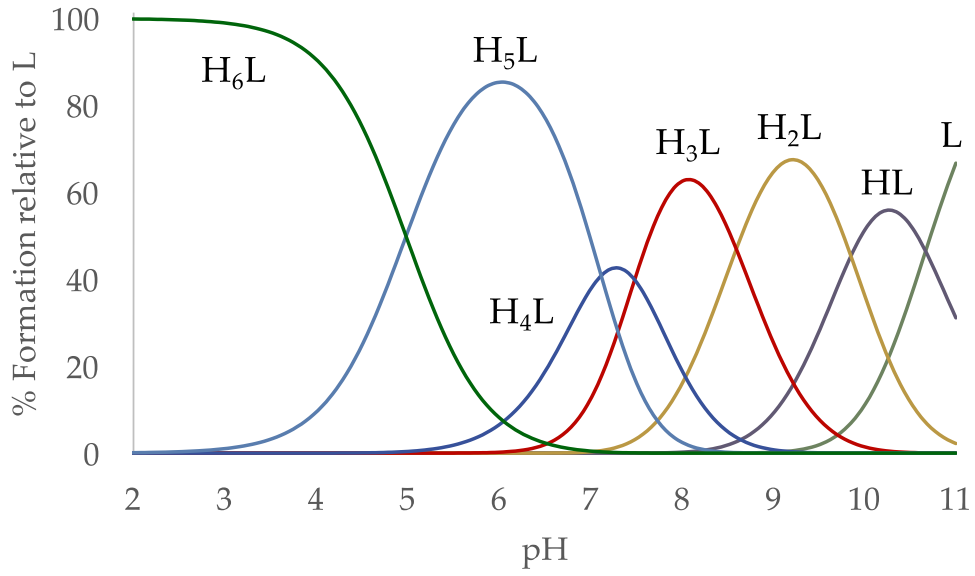

Figure S19. Distribution diagram of **L3** as a function of the pH in aqueous solution.

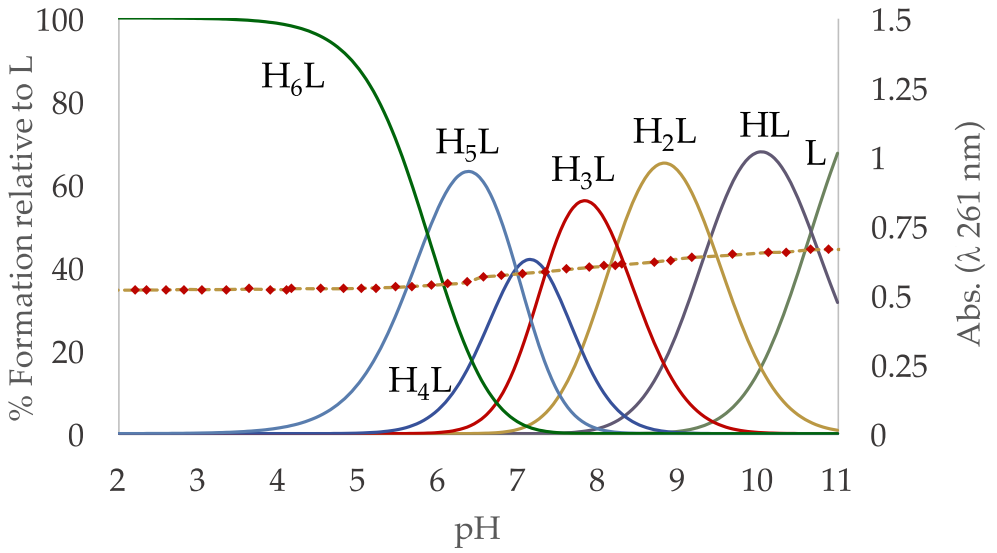

Figure S20. Distribution diagram of **L4** as a function of the pH in aqueous solution.

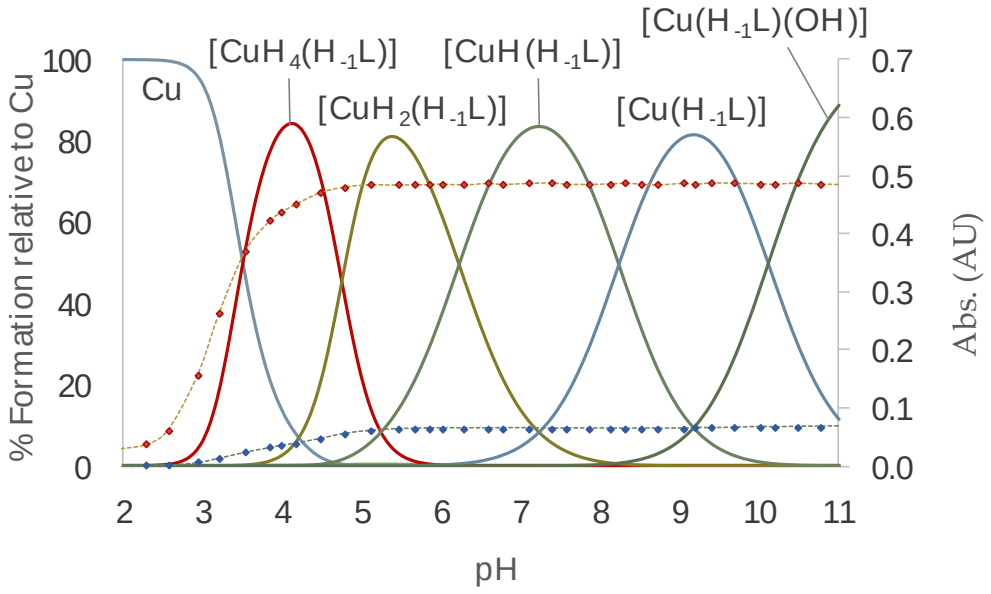

Figure S21. Distribution diagram of the Cu^{2+}:**L1** 1:1 system as a function of the pH in aqueous solution. The UV-Vis spectroscopic parameters of the pyridine system (red dots) and d-d transition band (blue dots) are overlaid.

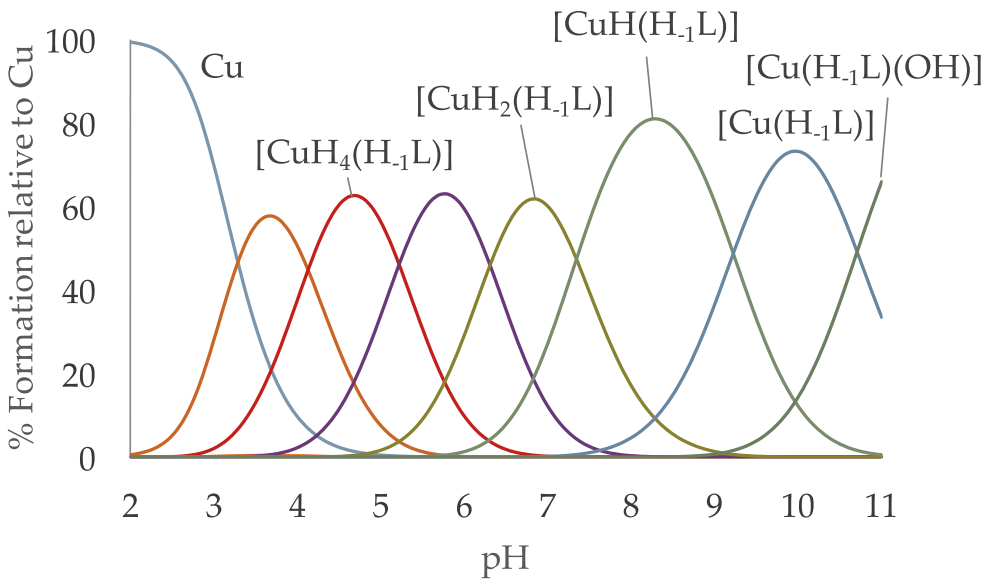

Figure S22. Distribution diagram of the Cu^{2+}:**L2** 1:1 system as a function of the pH in aqueous solution.

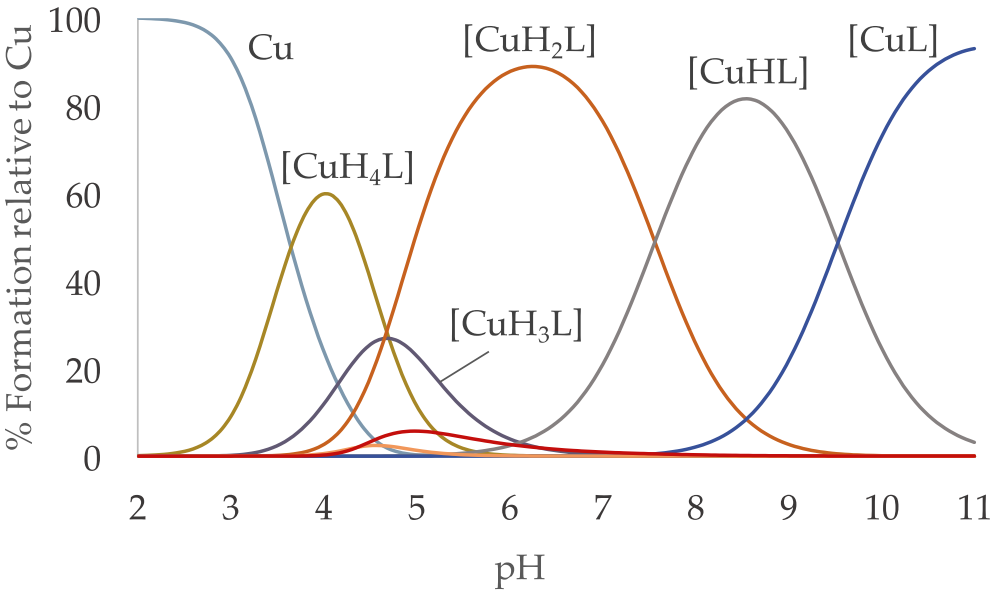

Figure S23. Distribution diagram of the Cu^{2+}:**L3** 1:1 system as a function of the pH in aqueous solution.

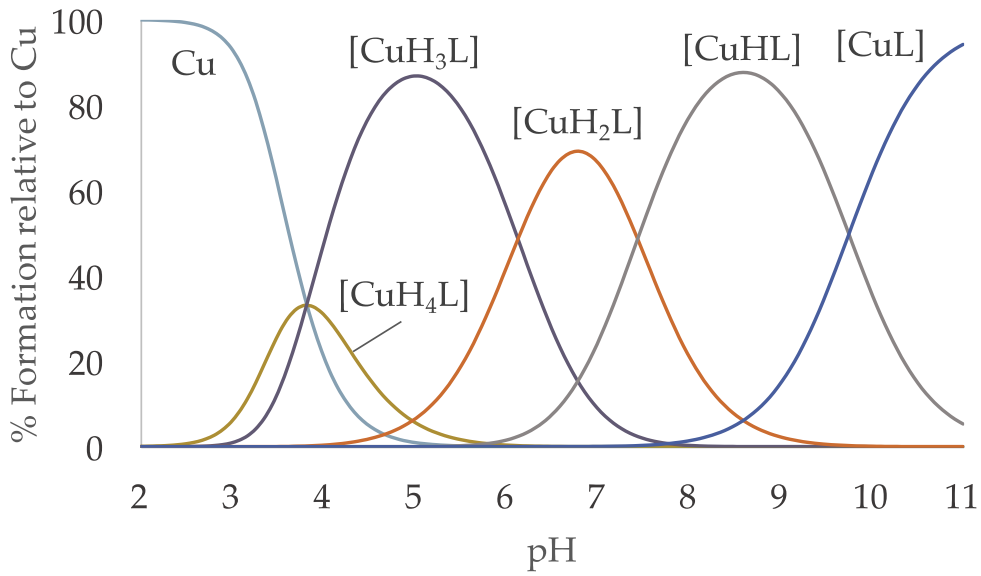

Figure S24. Distribution diagram of the Cu^{2+}:**L4** 1:1 system as a function of the pH in aqueous solution.

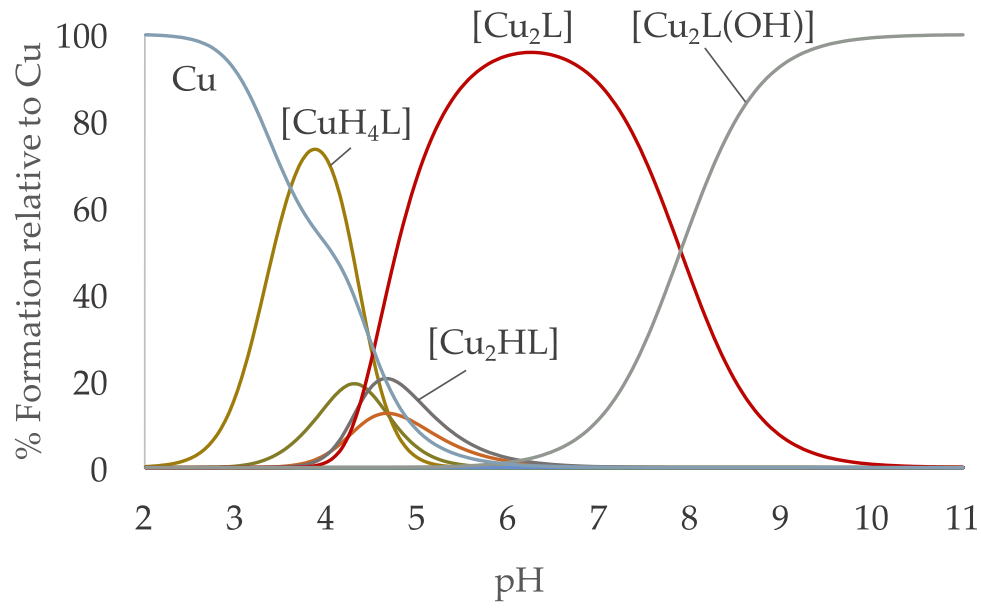

Figure S25. Distribution diagram of the Cu^{2+}:**L3** 2:1 system as a function of the pH in aqueous solution.

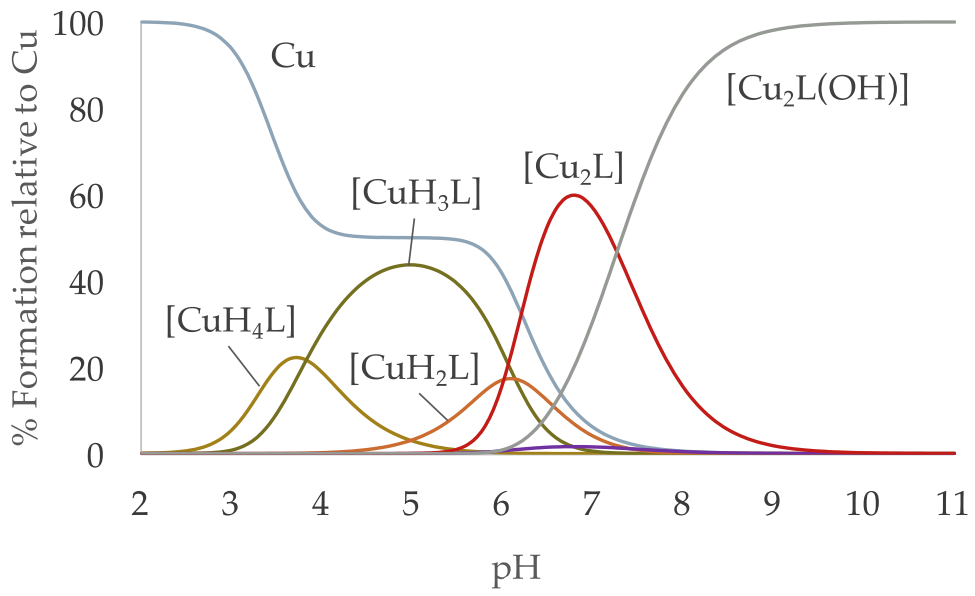

Figure S26. Distribution diagram of the Cu^{2+}:**L4** 2:1 system as a function of the pH in aqueous solution.

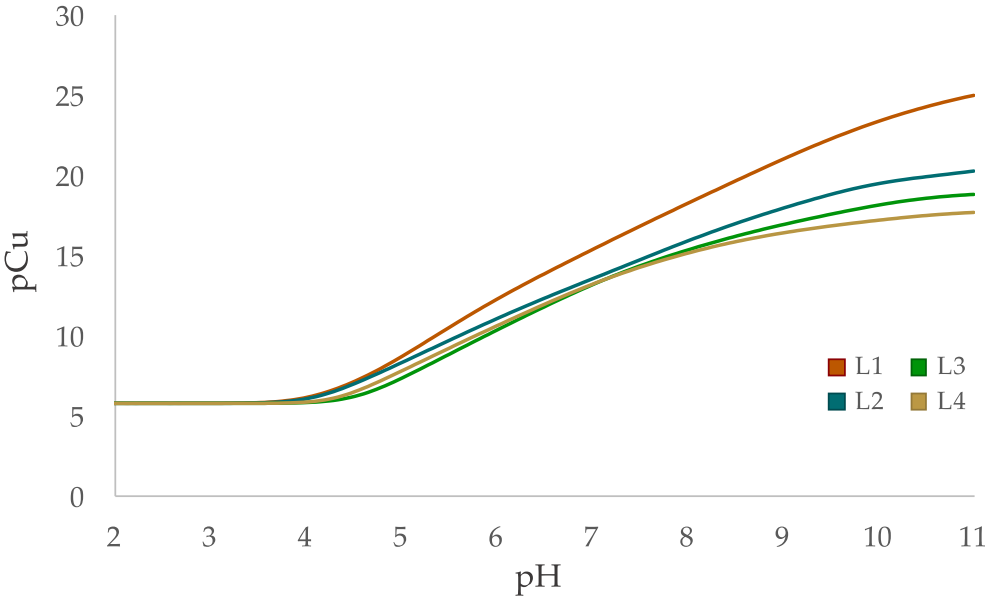

Figure S27. Representation of pCu^{2+} vs. pH for **L1** (brown line), **L2** (blue line), **L3** (green line) and **L4** (yellow line) ($[Cu^{2+}]_{tot} = 2 \cdot 10^{-6}$ M; $[L]_{tot} = 10^{-5}$ M).

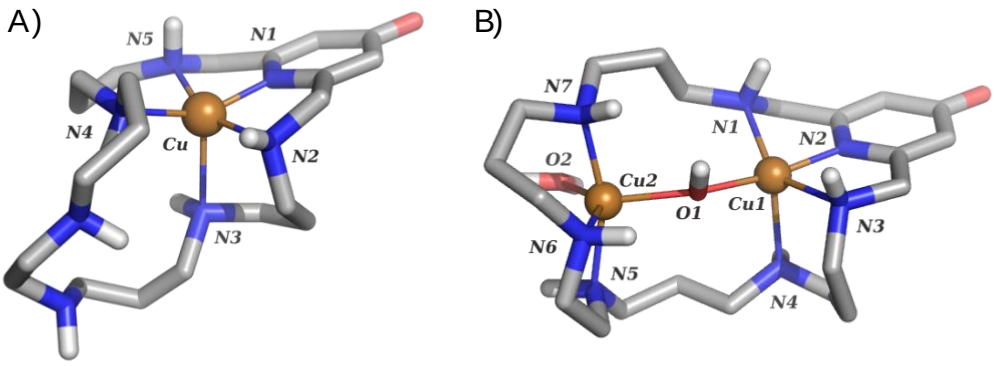

Figure S28. DFT optimized structure of Cu^{2+}:**L1** complex at physiological pH (7.40): A) Cu^{2+}:**L1** 1:1, B) Cu^{2+}:**L1** 2:1.

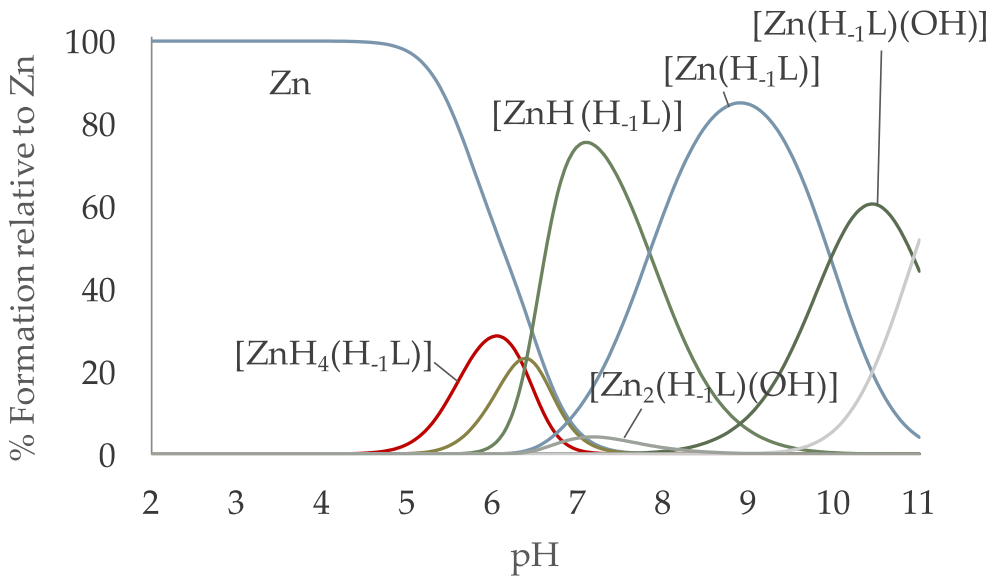

Figure S29. Distribution diagram of the Cu^{2+}:**L1** 1:1 system as a function of the pH in aqueous solution.

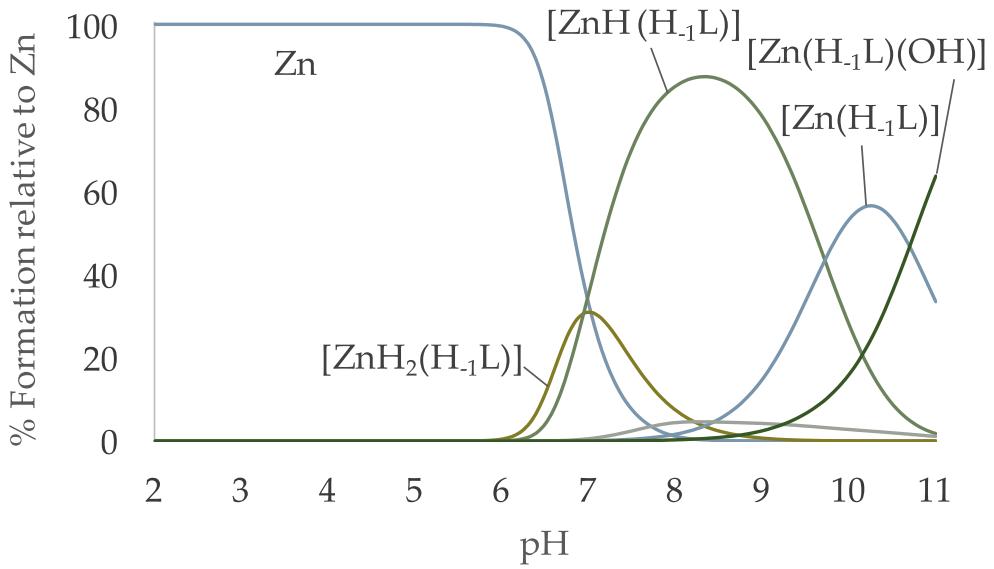

Figure S30. Distribution diagram of the Cu^{2+}:**L2** 1:1 system as a function of the pH in aqueous solution.

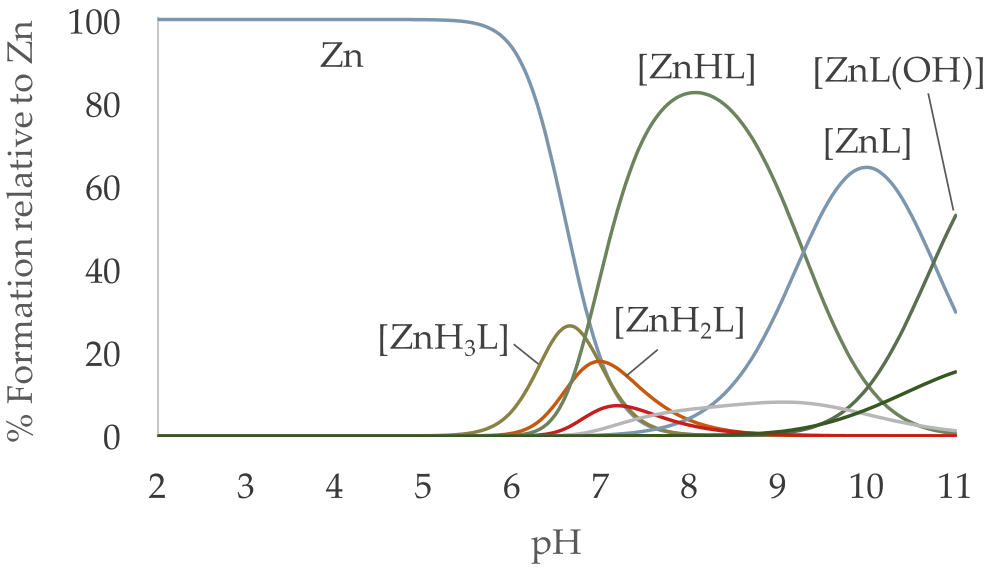

Figure S31. Distribution diagram of the Cu^{2+}:**L3** 1:1 system as a function of the pH in aqueous solution.

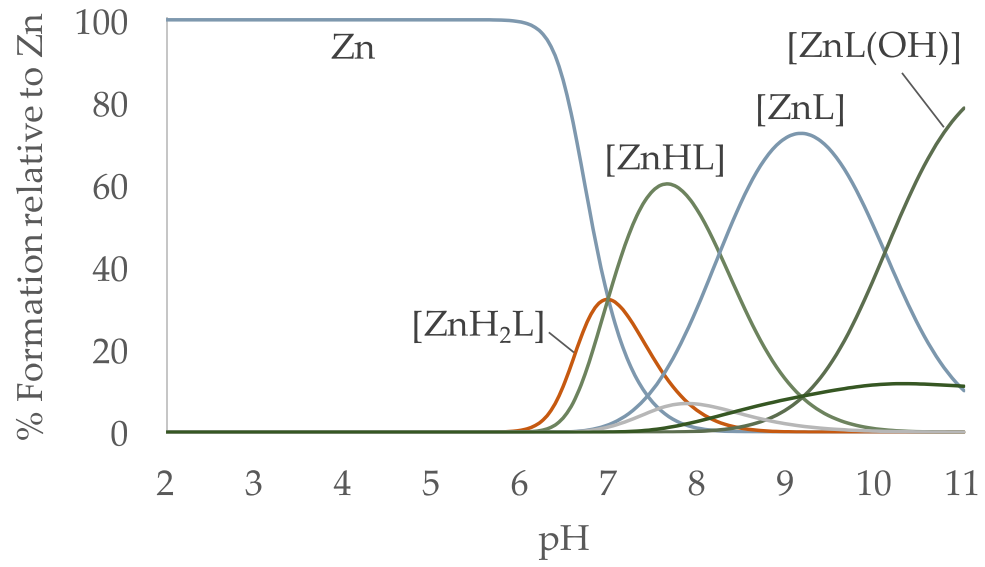

Figure S32. Distribution diagram of the Cu^{2+}:**L4** 1:1 system as a function of the pH in aqueous solution.

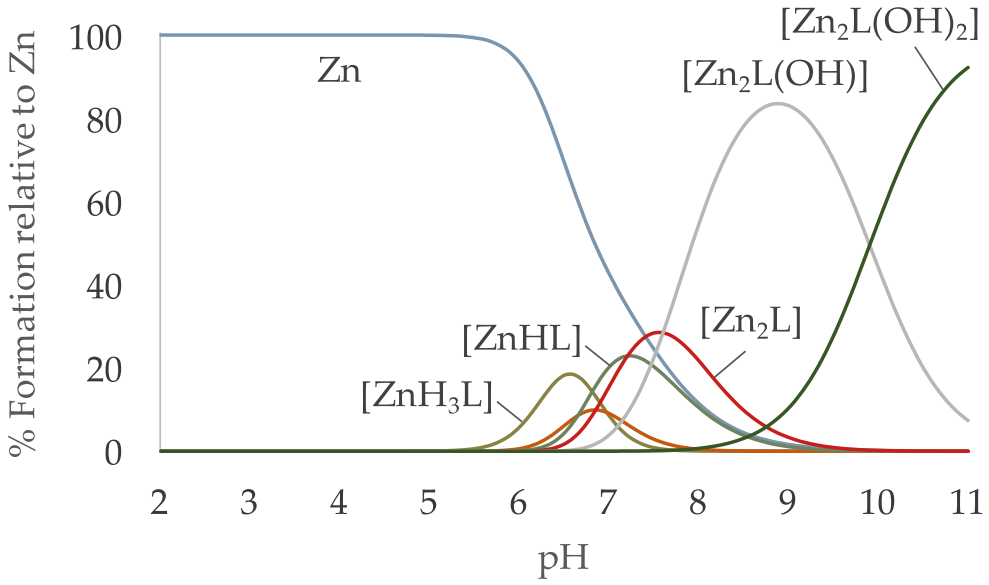

Figure S33. Distribution diagram of the Cu^{2+}:**L3** 2:1 system as a function of the pH in aqueous solution.

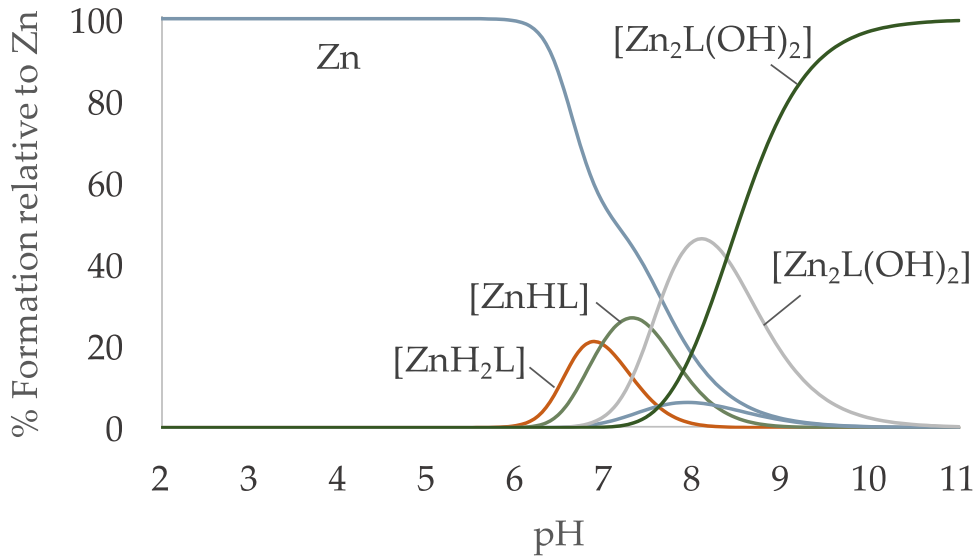

Figure S34. Distribution diagram of the Cu^{2+}:**L4** 2:1 system as a function of the pH in aqueous solution.

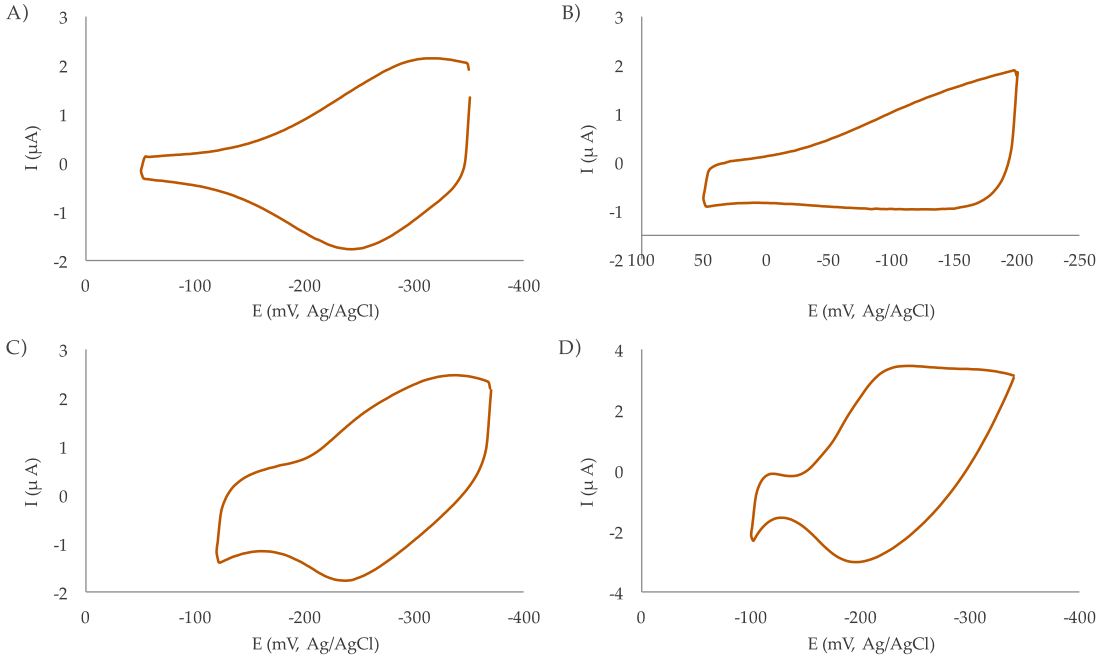

Figure S35. Cyclic voltammograms at glassy carbon electrode of 10^{-3} M solutions of A) Cu**L1**, B) Cu_2**L1**, C) Cu**L2**, D) Cu_2**L2** in 0.15 $NaClO_4$ aqueous solutions at pH 7.4. Potential scan rate 50 mV s^{-1}. Semi-derivative deconvolution of data was performed to increase peak resolution.

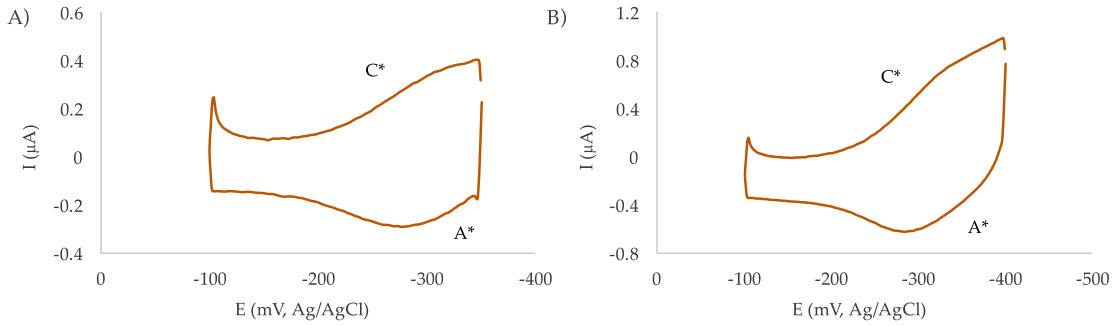

Figure S36. Cyclic voltammograms at glassy carbon electrode of 10^{-3} M solutions of Cu^{2+} (aq) plus **BNP-L2** in A) 1:1 and B) 2:1 molar ratios, in 0.15 $NaClO_4$ aqueous solutions at pH 7.4. Semi-derivative deconvolution of data was performed to increase peak resolution.

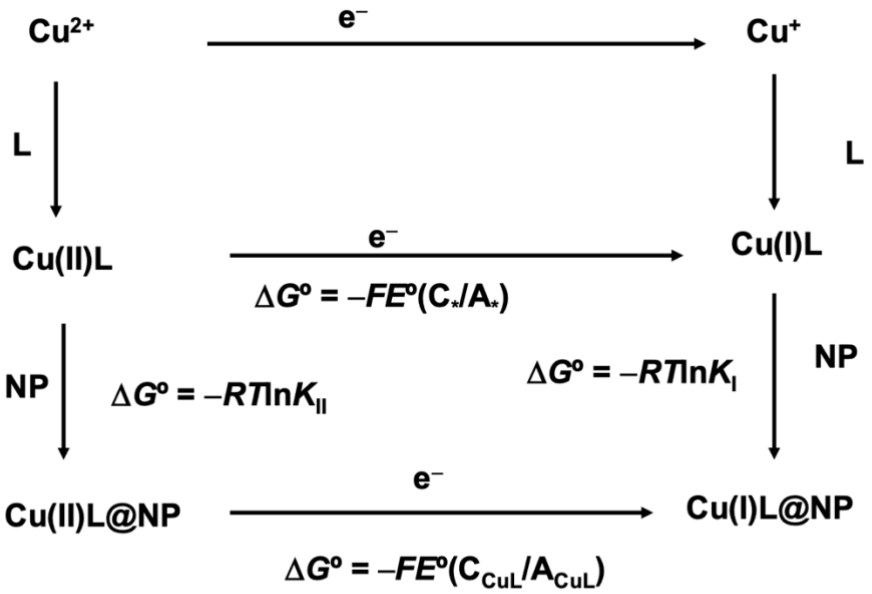

Figure S37. Thermochemical cycle for the NP-complex interaction and electrochemistry.

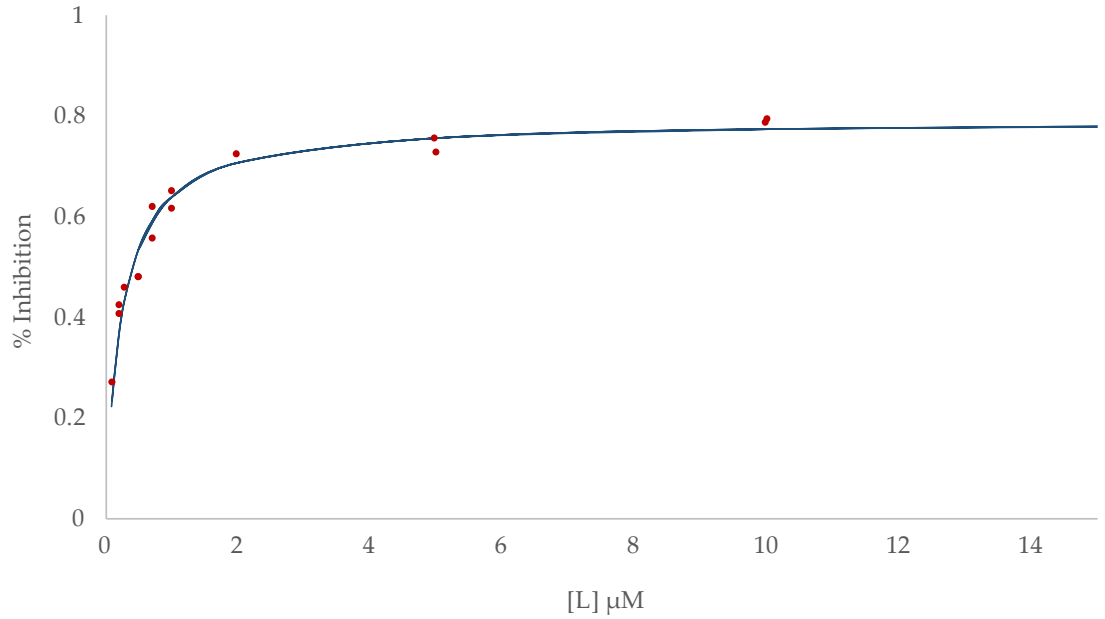

Figure S38. Fitting of the SOD activity data obtained by the McCord-Fridovich method for the system Cu_2-**L2**.

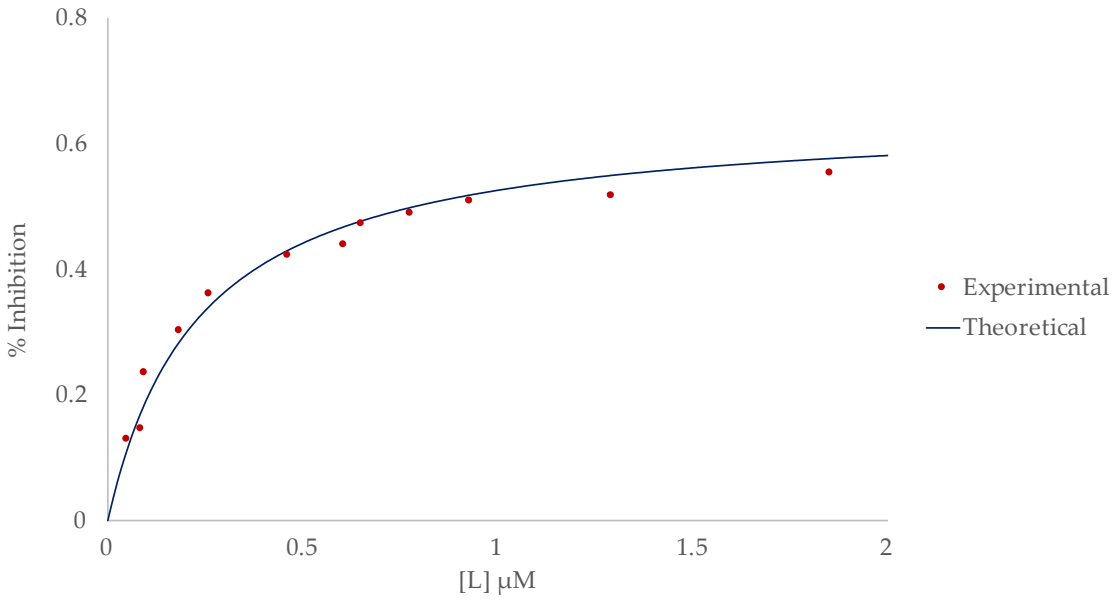

Figure S39. Fitting of the SOD activity data obtained by the McCord-Fridovich method for the system Cu_2-**BNP-L2**.

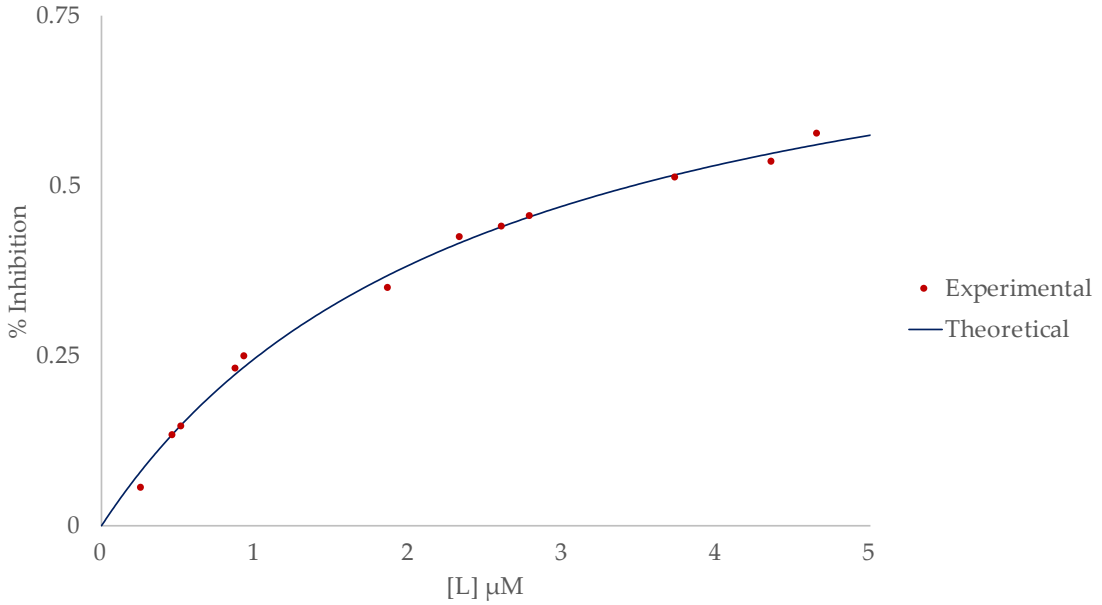

Figure S40. Fitting of the SOD activity data obtained by the McCord-Fridovich method for the system Cu_2-**SNP-L1**.

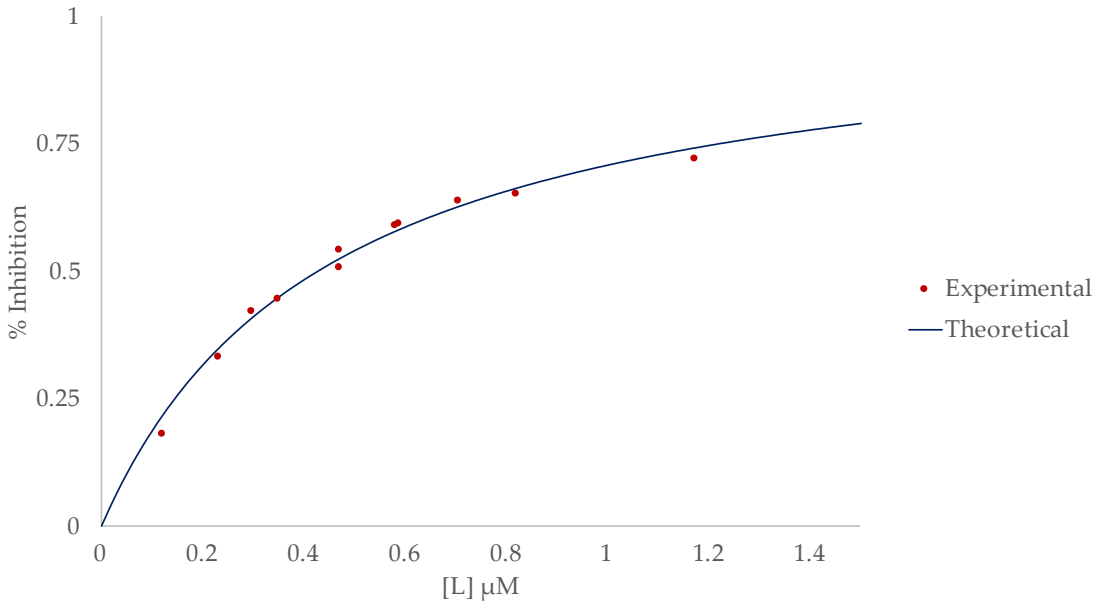

Figure S41. Fitting of the SOD activity data obtained by the McCord-Fridovich method for the system Cu_2-**SNP-L2**.

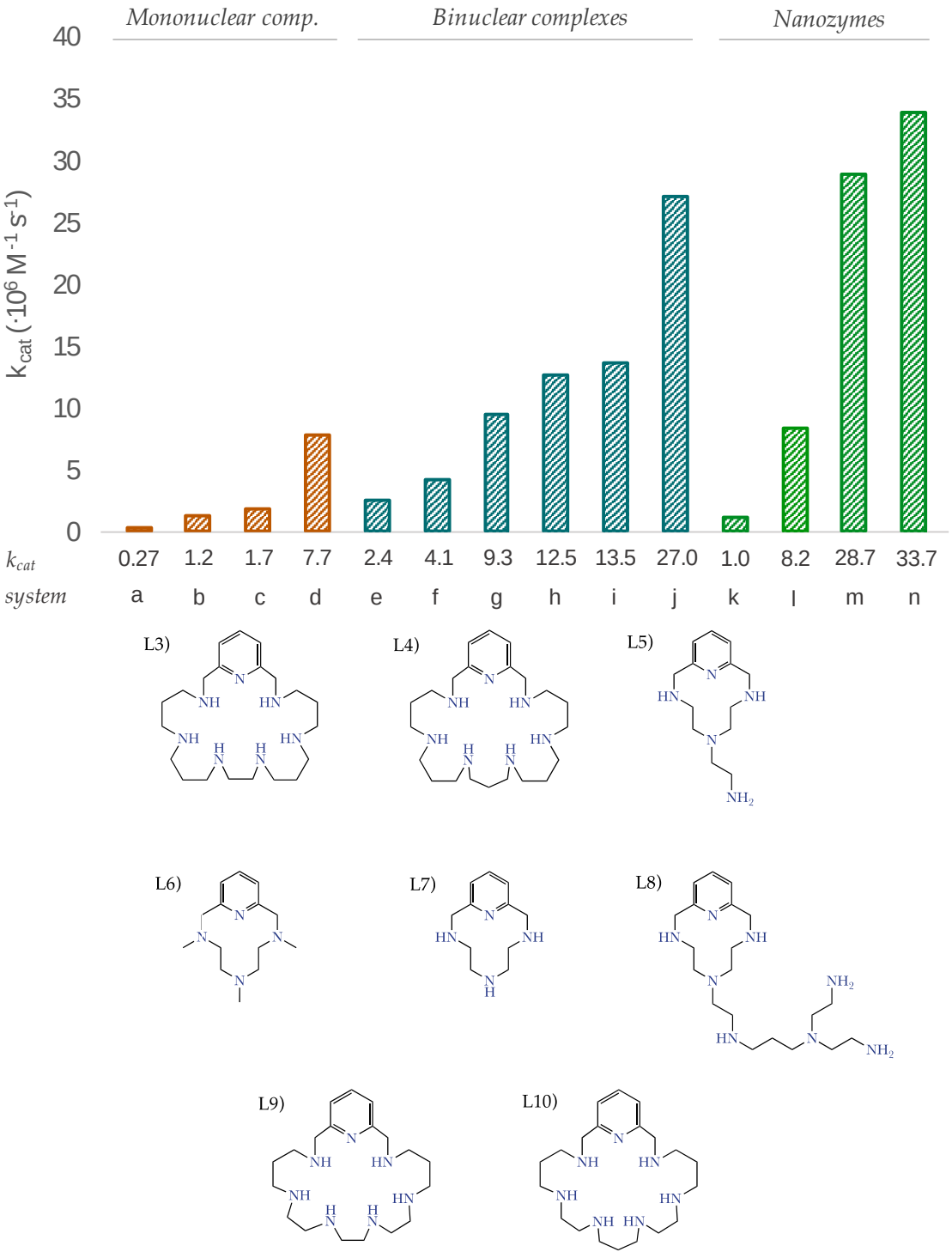

Figure S42. Representation of the catalytic constant corresponding to the systems: a) Cu-**L5**, Cu-**L6**, Cu-**L7**, Cu-**L8**, Cu_2-**L3**, Cu_2-**L1**, Cu_2-**L2**, Cu_2-**L9**, Cu_2-**L10**, Cu_2-**L4**, Cu_2-**SNP-L1**, Cu_2-**SNP-L2**, Cu_2-**BNP-L2**, Cu_2-**BNP-L1**.[1-3]

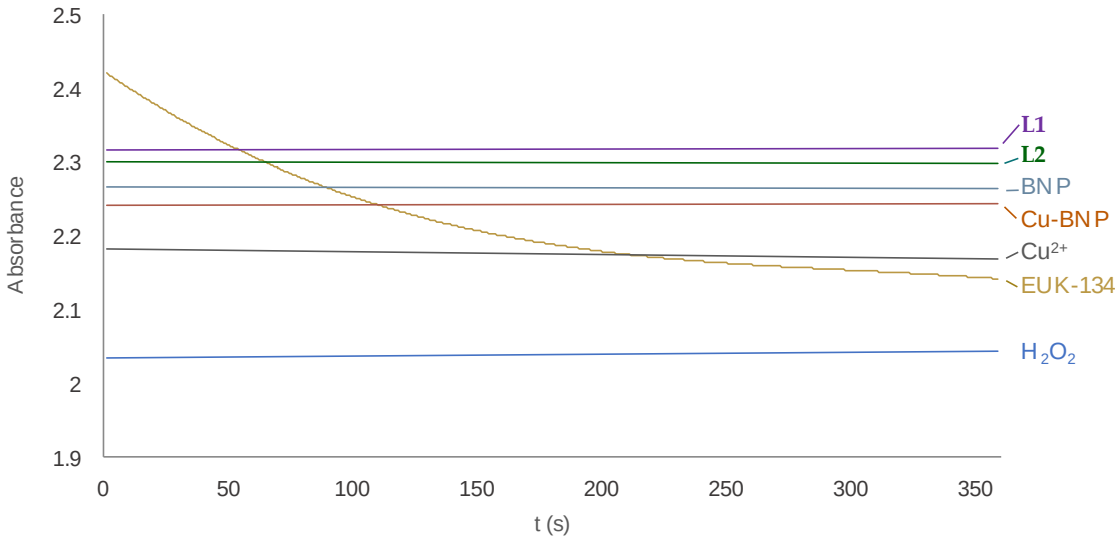

Figure S43. Representation of the variation of the absorbance intensity with time at 219 nm for H_2O_2 solutions with the presence of the ligands, both functionalised and free in solution. Yellow line corresponds to the EUK-134 reference.[4]

IV. Tables

Table S1. Concentration of the grafted ligand, Cu^{2+} complexation capability and ζ-potential values determined for the different nanoparticle systems. All measurements were carried out in 10^{-4} M $NaClO_4$ at pH 7.4.

System	[L] (mol/g_{NP})	[Cu^{2+}] (mol/g_{NP})	ζ-potential (mV)
BNP	-	-	32.1(8)
BNP-L1	3.5(4)·10-5	6.8(6)·10-5	23.9(2)
BNP-L2	2.20(2)·10-4	4.2(8)·10-4	35(2)
SNP	-	-	-18.1(9)
SNP-L1	2.3(2)·10-5	4.4(4)·10-5	-14.9(2)
SNP-L2	3.3(3)·10-5	6.0 (4)·10-5	-5.6(2)

a) Values in parenthesis are standard deviations in the last significant figure.

Table S2. Logarithms of the stepwise protonation constants for **L3** and **L4** obtained by potentiometric measurements.[1] The constants were determined in 0.15 M $NaClO_4$ at 298.1 ± 0.1 K.

Reaction	L3	L4
$L + H^+ \rightleftarrows HL^+$	10.67(1)	10.67(1)
$HL^+ + H^+ \rightleftarrows H_2L^{2+}$	9.85(1)	9.41(1)
$H_2L^{2+} + H^+ \rightleftarrows H_3L^{3+}$	8.60(1)	8.24(5)
$H_3L^{3+} + H^+ \rightleftarrows H_4L^{4+}$	7.49(1)	7.35(7)
$H_4L^{4+} + H^+ \rightleftarrows H_5L^{5+}$	7.12(1)	6.98(9)
$H_5L^{5+} + H^+ \rightleftarrows H_6L^{6+}$	4.99(2)	5.87(2)
log βb	48.72	48.52

a Values in parentheses are standard deviations in the last significant figure.
b $\text{Log } \beta = \sum \log K$

Table S3. Logarithm of the equilibrium constants for the interaction of Cu^{2+} with **L3** and **L4** obtained by potentiometric measurements.[1] The logarithms constants were determined in 0.15 M $NaClO_4$ at 298.1 ± 0.1 K.

Entry	Reaction	L3	L4
1	$[CuH_3L]^{5+} + H^+ \rightleftarrows [CuH_4L]^{6+}$	4.69(2)	3.82(2)
2	$[CuH_2L]^{4+} + H^+ \rightleftarrows [CuH_3L]^{5+}$	4.65(2)	6.13(2)
3	$[CuHL]^{3+} + H^+ \rightleftarrows [CuH_2L]^{4+}$	7.56(3)	7.44(2)
4	$[CuL]^{2+} + H^+ \rightleftarrows [CuHL]^{3+}$	9.53(3)	9.75(3)
5	$L + Cu^{2+} \rightleftarrows [CuL]^{2+}$	18.34(3)	17.22(6)
6	$[CuL]^{2+} + Cu^{2+} \rightleftarrows [Cu_2L]^{4+}$	11.69(3)	7.96(6)
7	$[Cu_2L]^{4+} + H_2O \rightleftarrows [Cu_2L(OH)]^{3+} + H^+$	-7.72(3)	-7.26(6)

[a] Values in parentheses are standard deviations in the last significant figure.

Table S4. Logarithms of the equilibrium constants for the interaction of Zn^{2+} with **L1**[2] and **L2** obtained by potentiometric measurements. The logarithms constants were determined in 0.15 M $NaClO_4$ at 298.1 ± 0.1 K.

Entry	Reaction	L1[3]	L2
1	$[ZnH_2(H_{-1}L)]^{3+} + H^+ \rightleftarrows [ZnH_3(H_{-1}L)]^{4+}$	6.32(3)	-
2	$[ZnH(H_{-1}L)]^{2+} + 2H^+ \rightleftarrows [ZnH_3(H_{-1}L)]^{4+}$	12.78(2)	-
3	$[ZnH(H_{-1}L)]^{2+} + H^+ \rightleftarrows [ZnH_2(H_{-1}L)]^{3+}$	-	6.96(3)
4	$[Zn(H_{-1}L)]^{+} + H^+ \rightleftarrows [ZnH(H_{-1}L)]^{2+}$	7.83(1)	9.76(2)
5	$Zn^{2+} + H_{-1}L^{-} \rightleftarrows [Zn(H_{-1}L)]^{+}$	14.65(2)	9.84(6)
6	$[Zn(H_{-1}L)]^{+} + H_2O \rightleftarrows [Zn(H_{-1}L)(OH)] + H^+$	-9.96(3)	-
7	$[Zn(H_{-1}L)(OH)] + H_2O \rightleftarrows [Zn(H_{-1}L)(OH)_2]^{-} + H^+$	-10.93(3)	-
8	$2Zn^{2+} + [(H_{-1}L)]^{+} + H_2O \rightleftarrows [Zn_2(H_{-1}L)(OH)]^{2+} + H^+$	11.14(2)	6.71(6)
9	$2Zn^{2+} + [(H_{-1}L)]^{+} + 2H_2O \rightleftarrows [Zn_2(H_{-1}L)(OH)2]^{2+} + H^+$	2.33(3)	-3.03(6)
10	$2Zn^{2+} + [(H_{-1}L)]^{+} + 3H_2O \rightleftarrows [Zn_2(H_{-1}L)(OH)3]^{+} + H^+$	-7.92(4)	
11	$Zn^{2+} + [Zn(H_{-1}L)]^{+} + H_2O \rightleftarrows [Zn_2(H_{-1}L)(OH)]^{2+} + H^+$	-3.51(3)	-3.13(3)
12	$[Zn_2(H_{-1}L)(OH)]^{2+} + H_2O \rightleftarrows [Zn_2(H_{-1}L)(OH)_2]^{+} + H^+$	-8.81(3)	-9.74(6)
13	$[Zn_2(H_{-1}L)(OH)_2]^{2+} + H_2O \rightleftarrows [Zn_2(H_{-1}L)(OH)_3] + H^+$	-10.25(4)	-

[a] Values in parentheses are standard deviations in the last significant figure.

Table S5. Logarithm of the equilibrium constants for the interaction of Zn^{2+} with **L3** and **L4** obtained by potentiometric measurements.[1] The logarithms constants were determined in 0.15 M $NaClO_4$ at 298.1 ± 0.1 K.

Entry	Reaction	L3	L4
1	$[ZnH_2L]^{4+} + H^+ \rightleftarrows [ZnH_3L]^{5+}$	6.97(4)	-
2	$[ZnHL]^{3+} + H^+ \rightleftarrows [ZnH_2L]^{4+}$	6.65(6)	6.99(3)
3	$[ZnL]^{2+} + H^+ \rightleftarrows [ZnHL]^{3+}$	9.28(3)	8.24(4)
4	$Zn^{2+} + L \rightleftarrows [ZnL]^{2+}$	10.76(4)	10.32(4)
5	$Zn^{2+} + L + H_2O \rightleftarrows [ZnL(OH)]^{+} + H^+$	0.01(5)	0.21(6)
6	$[ZnL]^{2+} + H_2O \rightleftarrows [ZnL(OH)]^{+} + H^+$	-10.75(7)	-10.11(7)
7	$2Zn^{2+} + L \rightleftarrows [Zn_2L]^{4+}$	15.69(5)	-
8	$Zn^{2+} + [ZnL]^{2+} \rightleftarrows [Zn_2L]^{4+}$	4.93(6)	-
9	$2Zn^{2+} + L + H_2O \rightleftarrows [Zn_2L(OH)]^{3+} + H^+$	8.10(2)	6.36(6)
10	$2Zn^{2+} + L + 2H_2O \rightleftarrows [Zn_2L(OH)_2]^{2+} + H^+$	-1.80(2)	-2.03(1)
11	$[Zn_2L]^{4+} + H_2O \rightleftarrows [Zn_2L(OH)]^{3+} + H^+$	-7.59(5)	-
12	$[Zn_2L(OH)]^{3+} + H_2O \rightleftarrows [Zn_2L(OH)_2]^{2+} + H^+$	-9.90(3)	-8.39(6)

[a] Values in parentheses are standard deviations in the last significant figure.

Table S6. Logarithm of the equilibrium constants for the interaction of Cu^{2+} and Zn^{2+} with **L3** and **L4** obtained by potentiometric measurements.[1] The logarithms constants were determined in 0.15 M $NaClO_4$ at 298.1 ± 0.1 K.

Entry	Reaction	L3	L4
4	$[CuZnL]^{4+} + H^+ \rightleftarrows [CuZnHL]^{5+}$	-	30.23(6)
5	$Cu^{2+} + Zn^{2+} + L \rightleftarrows [CuZnL]^{4+}$	23.26(9)	-
6	$Cu^{2+} + Zn^{2+} + L + H_2O \rightleftarrows [CuZnL(OH)]^{3+} + H^+$	18.57(2)	14.55(3)
7	$Cu^{2+} + Zn^{2+} + L + 2H_2O \rightleftarrows [CuZnL(OH)_2]^{2+} + 2H^+$	5.34(6)	6.24(3)

[a] Values in parentheses are standard deviations in the last significant figure.

IV. References

1 R. Belda, S. Blasco, B. Verdejo, H. R. Jiménez, A. Doménech-Carbó, C. Soriano, J. Latorre, C. Terencio and E. García-España, *Dalton Trans.*, 2013, **42**, 11194.

2 Á. Martínez-Camarena, E. Delgado-Pinar, C. Soriano, J. Alarcón, J. M. Llinares, R. Tejero and E. García-España, *Chem. Commun.*, 2018, **54**, 3871.

3 L. Guijarro, M. Inclán, J. Pitarch-Jarque, A. Doménech-Carbó, J. U. Chicote, S. Trefler, E. García-España, A. García-España and B. Verdejo, Inorg. Chem., 2017, **56**, 13748.

4 I. Ivanović-Burmazović and M. R. Filipović, *Adv. Inorg. Chem.*, 2012, **64**, 53.